Available online at www.sciencedirect.com

SciVerse ScienceDirect

Ceramics International 38 (2012) 3885–3892

CERAMICS INTERNATIONAL

www.elsevier.com/locate/ceramint

A comprehensive study on the magnetic properties of nanocrystalline $SrCo_{0.2}Fe_{11.8}O_{19}$ ceramics synthesized via diverse routes

Y. Ebrahimi [a,b], A.A. Sabbagh Alvani [b,*], A.A. Sarabi [a], H. Sameie [a,b], R. Salimi [a,b], M. Sabbagh Alvani [c], S. Moosakhani [a,b]

[a] Faculty of Polymer Engineering & Color Tech., Amirkabir University of Technology, P.O. Box 15875-4413, Tehran, Iran
[b] Color and Polymer Research Center (CPRC), Amirkabir University of Technology, P.O. Box 15875-4413, Tehran, Iran
[c] Faculty of Materials Science & Engineering, University of New South Wales, Sydney, NSW 2052, Australia

Received 14 November 2011; received in revised form 11 January 2012; accepted 17 January 2012
Available online 25 January 2012

Abstract

The effects of the synthesis techniques: sol–gel combustion (SG), hydrothermal (HT) and co-precipitation (CP) on the structure, homogeneity, morphology and magnetic properties of $SrCo_{0.2}Fe_{11.8}O_{19}$ hexaferrite ceramics have methodically been explored by X-ray diffraction (XRD), laser particle analyzer, scanning electron microscopy (SEM) and vibrating sample magnetometer (VSM). Structural analysis results revealed that the variety of the synthesis techniques evidently reflects variation in the lattice parameters and grain sizes. Moreover, diverse morphologies such as lamellar, disc-like and needle-shape for SG, HT and CT routes were observed, respectively. The maximum saturation magnetization (31.2 emu/g) and coercivity (4950 Oe) belonged to the co-precipitation technique owning to its higher phase purity, more homogeneity and larger crystalline size. Apparently, the softer ferrites were attainable by hydrothermal and sol–gel combustion routes, whereas, the co-precipitation technique led to harder magnets.

Keywords: C. Magnetic properties; Hexaferrite ceramic; Nanocrystalline; Synthesis method

1. Introduction

M-type hexagonal ferrites have emerged as novel materials with vast technological and scientific interest considering their brilliant physical properties such as reliable magnetization, high coercive force, large magnetocrystalline anisotropy and relatively high Curie temperature, as well as remarkable chemical stability and low cost [1–3]. A great diversity of various cation substitutions are possible in M-type hexagonal ferrites which might be conveniently classified according to whether or not there is a necessity for charge compensation. Charge compensation is not required when direct isovalent substitution is made. Nonetheless, it is recurrently desired to substitute divalent transition metals such as Cu(II), Ni(II) and Co(II) for Fe(III) due to their similar ionic radii [3–6]. Co-substitution is also found to produce disorder and oxygen vacancies in the hexaferrite structure [7–10]. It has been reported that the magnetic moment of Co^{2+} is 3.7 μB and its ions have preferential occupancy of $4f_1$–$4f_2$ sites with d^7 configuration [11], while Wiesinger et al. [12] and Lechevallier et al. [13] reported that Co^{2+} ions have a noticeable preference for octahedral sites, being substituted for Fe^{3+} in both $4f_2$ and 2a sites. It is reasonable then to assume that the smaller magnetic moment of Co^{2+} is responsible for the super-exchange that gives rise to a nearly decrease in Ms which is further related to low magnetic moment of Co^{2+} ions to Fe^{3+} ions (5 μB) [14]. In M-type hexagonal ferrite, the Co(II) ion was singled out for cation substitution since it is famed for giving strong planar contribution to the anisotropy of the magnetic structure [15–17]. However so far, none has been fully characterized its magnetic properties in Sr hexagonal ferrite via different methods. In nano scale materials, physical, chemical and magnetic properties are size dependant. In order to tune these properties, various groups have been working on optimizing particle size and the other features by varying synthesis routes and processes [18–21]. Furthermore, the magnetic properties

* Corresponding author. Tel.: +98 21 66418600; fax: +98 21 66418601.
E-mail address: sabbagh_alvani@aut.ac.ir (A.A. Sabbagh Alvani).

0272-8842/$36.00
doi:10.1016/j.ceramint.2012.01.040

depend mostly on the grain size and phase purity which are very much affected by the kind of synthesis [3]. Hence, strontium hexagonal ferrites have been produced by numerous processes such as co-precipitation, solid state reaction, hydrothermal synthesis, sol–gel techniques, micro-emulsion, salt-melt technique and citrate sol–gel combustion route and etc., which vary in the cost and product properties [22–30]. The conventional way of synthesizing hexaferrites involves solid state reaction route necessitates high calcination temperature ($\geq$1200 °C), which leads to powders with large particle size require further extensive processing, limited chemical homogeneity, low sinterability, high capital investment and high-energy consumption [31]. However, most of wet-chemical methods have a few pitfalls like complex equipment and expensive precursors in addition to the disposal of the by-product which the citrate sol–gel combustion and the hydrothermal methods seldom would suffer from [18,32,33]. Among these reproducible synthesis routes, co-precipitation technique is one of the most appropriate and versatile methods owing to its high homogeneity and purity [3,19,24]. To explore every avenue towards, the main aim of this study was to develop a synthesis of nanocrystalline $SrCo_{0.2}Fe_{11.8}O_{19}$ powders corresponding to the stoichiometry via the citrate sol–gel combustion, hydrothermal and co-precipitation techniques and analysing their structural, morphological and magnetic properties as well.

2. Experimental procedure

Ferrite materials are regularly prepared by three techniques: citrate sol–gel combustion technique, co-precipitation method and hydrothermal technique, in order to make a comparison between the estimated structure parameters, which affect the particle size, the microstructure and the magnetic properties of co-substituted strontium hexagonal ferrites. In all studies, the reactants were dissolved in deionized water, and then NaOH was added two times in excess. A schematic diagram of the synthesis processes is displayed in Fig. 1.

2.1. Preparation techniques

2.1.1. Co-precipitation method

Chemically grade ferric chloride nitrate $Fe(NO_3)_3{\cdot}9H_2O$, strontium nitrate $Sr(NO_3)_2$, $Co(NO_3)_2{\cdot}6H_2O$ and sodium hydroxide (NaOH) were used as raw materials. The ferrite precursors were precipitated from theses mixtures by adding gradually sodium hydroxide (5 M) solution as a co-precipitation agent at room temperature at pH 11. The aqueous suspensions were stirred gently for 20 min to achieve good homogeneity and to attain stable pH conditions. After precipitation, the resulted gel like cake was thoroughly washed with deionized water and purified with ethanol. The washed $SrCo_{0.2}Fe_{11.8}O_{19}$ powders were dried at 100 °C and then calcined at 800 °C for 1 h.

2.1.2. Citrate sol–gel combustion method

$Fe(NO_3)_3{\cdot}9H_2O$, $Co(NO_3)_2{\cdot}6H_2O$ and $Sr(NO_3)_2$, in a molar ratio of 11.8 were dissolved in deionized water. Citric acid was dissolved into the solutions to give a molar ratio of metal ions to citric acid as a fuel of 1:1 and the solutions were allowed several minutes to return to room temperature and the solution became clear and homogeneous. The molar ratio of citric acid to the metal nitrate (CA/MN) of 1.5 was then added into the prepared aqueous solution to chelate Fe^{3+} and Sr^{2+}. In addition, proper amount of sodium hydroxide was added to adjust pH at 7. The homogenous solution was slowly evaporated under stirring condition on a hot plate to obtain their gels. As water evaporated, the solutions became viscous and finally formed very viscous brown gels. With temperature increasing, the gel burnt in a self-propagating combustion manner until gels were burnt completely to form a loose powder. The resulting dark brown ashes were calcined at 800 °C for 1 h.

2.1.3. Hydrothermal method

The starting materials used for these experiment were $Fe(NO_3)_3{\cdot}9H_2O$, $Sr(NO_3)_2$, $Co(NO_3)_2{\cdot}6H_2O$ and NaOH. The

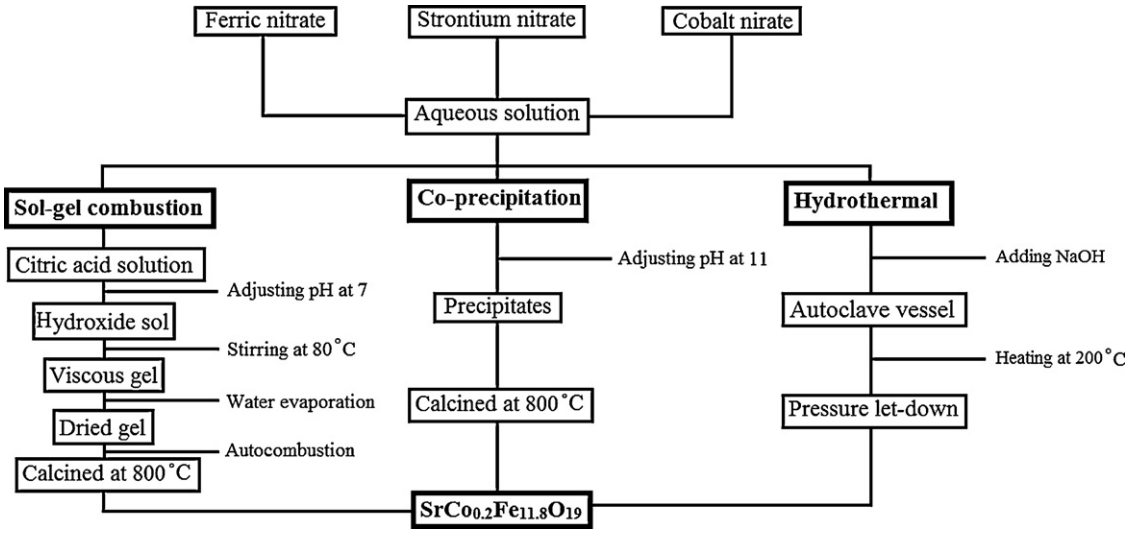

Fig. 1. Schematic diagram of synthesis routes.

resulting suspension was sealed in an autoclave cell and heated at rate of 10 °C/min to 200 °C and then cooled to room temperature to produce precipitated slurry which was then filtered and washed repeatedly using deionized water until no Cl^- was detectable and then dried at 100 °C in an oven.

2.2. Characterization techniques

2.2.1. XRD analysis

The resulting powders were analyzed by X-ray diffraction (XRD) with Bruker AXS: D8 ADVANCE. This instrument works with voltage and current settings of 40 kV and 30 mA, respectively and uses Cu Kα radiation (1.5405 Å). For qualitative analysis, XRD diagrams were recorded in the interval $20^\circ \leq 2\theta \leq 70^\circ$ at scan speed of 2°/min.

2.2.2. Scanning electron microscopy (SEM)

The powders were coated with a thin layer of gold (Au) by sputtering (EMITECH K450X, England) and then the microstructure of them was observed in a scanning electron microscope (SEM; Stereoscan S 360 Cambridge) that operated at an acceleration voltage of 10 kV.

2.2.3. Particle size distribution (PSD)

Particle size distribution study of the prepared samples was carried out by using a laser particle size analyser Master sizer 2000. The samples were exposed to ultrasonic waves for 15 min before being analyzed. The samples were dispersed in ethanol suspension.

2.3. Vibrating sample magnetometer (VSM)

Magnetic properties were measured by a vibrating sample magnetometer (VSM) with a maximum applied field of 1100 kA/m.

3. Results and discussion

3.1. XRD analysis

The XRD diffraction patterns of $SrCo_{0.2}Fe_{11.8}O_{19}$ powders obtained by various methods are presented in Fig. 2(a)–(c) for samples obtained via CP, HT and SG methods, respectively. The hexagonal ferrite structure of $SrFe_{12}O_{19}$ (*P*63/*mmc*), which was described in JCPDS file number 33-1340, was detected in all three samples. In this pattern the presence of the hexagonal ferrite phase can be identified by peaks at 2θ 30.32° (1 1 0), 32.35° (1 0 7) and 34.18° (1 1 4). As it can be observed, the widths of the CP ferrite main peaks decreased in comparison with the HT and the SG peaks respectively, suggesting the suitable growth of the particles prepared by co-precipitation method. In the CP samples the peaks corresponding to the (1 0 7) and (1 1 4) directions sharpened, corresponding to an increase in domain size in these directions. The XRD phase-analysis also suggested that SG sample product comprised both $SrFe_2O_4$ and α-Fe_2O_3 phases as impurities probably due to the local combustion while preparation of samples via HT route

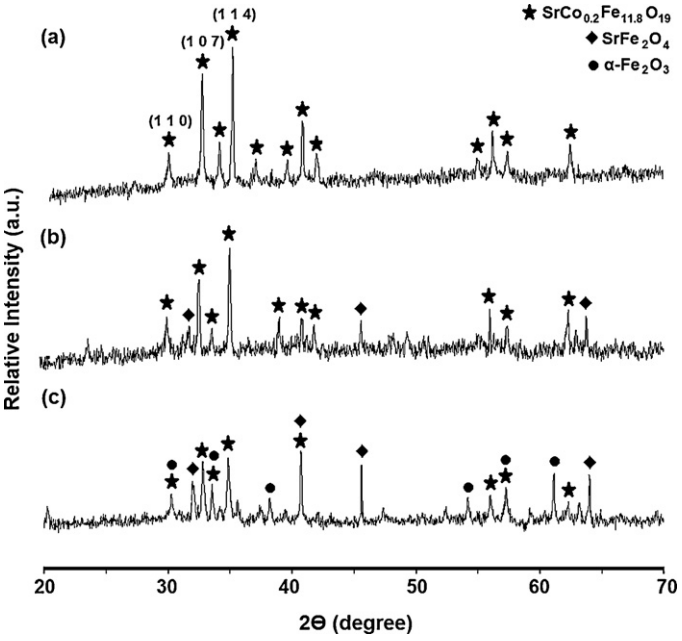

Fig. 2. XRD patterns of $SrCo_{0.2}Fe_{11.8}O_{19}$ nanocrystallites produced by co-precipitation (a), hydrothermal (b) and sol–gel combustion (c) methods.

revealed considerable formation of $SrFe_{12}O_{19}$ phase and traces of $SrFe_2O_4$ phase. Since pure mono-phasic $SrFe_{12}O_{19}$ obtained by CP route, it proposes this method as a promising route in order to prepare pure nanocrystalline hexagonal ferrite.

The crystalline size was estimated from the broadening of the peaks using the Scherrer's formula:

$$D_{hkl} = \frac{k\lambda}{\beta \cos\theta} \tag{1}$$

where β is the width of the pure diffraction profile in radians, k is 0.89, λ is the wavelength of the X-rays, θ is the diffraction angle, and $D_{h\,k\,l}$ is the average diameter of the crystallite. For this purpose, the strongest diffraction Bragg peak (1 1 4) is used to estimate the crystallite size of the samples. As it can be resulted from Table 1, the grain size of the samples is found to be in the range of 44–53 nm. Subsequently, the lattice constants a and c were calculated using the published Miller indices (h, k and l) of the reflections and their measured angular positions according to equation:

$$\frac{1}{d_{hkl}^2} = \frac{4}{3}\left(\frac{h^2 + hk + k^2}{a^2}\right) + \frac{l^2}{c^2} \tag{2}$$

Additionally, the X-ray densities were calculated as follows:

$$d_{\text{X-ray}} = \frac{2M}{N_A V_{\text{cell}}} \tag{3}$$

$$V_{\text{cell}} = \frac{\sqrt{3}}{2} a^2 c \tag{4}$$

where M is the molecular weight, V_{cell} is the cell volume, N_A denotes Avogadro number and finally a and c are lattice constants. Lattice parameters (a, c and V_{cell}) and X-ray densities

Table 1
Summary of powder X-ray diffraction measurements and average crystallite size for samples.

Method	a (±0.001 Å)	c (±0.001 Å)	V_{cell} (±2 Å^3)	$d_{X\text{-}ray}$ (g/cm^3)	Average grain size (nm)
SG	5.74	23.33	666	5.30	44
HT	5.87	23.20	693	5.09	46
CP	5.91	23.07	698	5.05	53

of the series $SrCo_{0.2}Fe_{11.8}O_{19}$ are also tabulated in Table 1. It demonstrates that the variations of synthesis method slight on lattice constants, cell volumes and densities of HT and CP compounds, whereas for SG samples the differences are distinctive.

3.2. SEM observations

The morphological characteristics of the obtained $SrCo_{0.2}Fe_{11.8}O_{19}$ were investigated by SEM analysis. Fig. 3 illustrates SEM micrographs of the samples prepared by co-precipitate method. As it can be observed, the particles seem to have needle-like shaped morphology with particle size less than 10 μm. Besides, the grains are distributed rather homogeneously without massive agglomerations.

Fig. 4 implies the representative SEM micrographs for $SrCo_{0.2}Fe_{11.8}O_{19}$ nanocrystallines prepared by citrate sol–gel route. The particles possessed a lamellar structure which presumably the pore walls shaped this structure when the sol was turned into the gel because of evaporation of a large amount of water [18]. On the other hand, careful observation on the particles' morphologies reveals that there are some aggregates and partially sintered microstructures. The combustion reaction was characterized as a fast process with abrupt ascent and descent of temperature which this phenomenon may have caused the crystallites of the product to possess the residual stress as well as crystal imperfections such as deficient crystallinity, oxygen vacancies, grain boundary defects, and interfacial dislocation pile-ups [34,35]. This agglomerated structure will complicate the study of the magnetic material owing to the interactions between the neighboring particles. At the same time, the distinguishable microscopic pores that affect the magnetic properties of the material are associated with the liberation of a large amount of gaseous materials.

Fig. 5 depicts that the hydrothermally synthesized particles have a disk-like shape with grains between 10 and 15 μm. Moreover, the grains are distributed rather homogenously without significant agglomerations.

In general, the results prove that the type of synthesis route converts the shape of particles and can effectively control the product size. Indeed, one can say that the powder microstructure depends considerably on the preparation technique.

3.3. Particle size distribution

Particle size distribution of all the samples is obtained by the laser particle size analyzer. The results signify that the particles prepared by co-precipitation method are more uniform and have a narrower distribution size. The majority of particles (90%) are less than 39 μm in size. This value is 43 and 44 μm for HT and SG derived samples, respectively. Generally, the mean particle size of all samples ranges from 17 to 20 μm which is consistent with the SEM observations. The approximated mean particle sizes of all the samples are larger than the crystallite size estimated by X-ray diffraction analysis. This can be explained regarding the following facts: (1) X-rays can only detect the crystallites, i.e. the well-ordered parts of the crystallites, and they cannot identify the disordered grain boundaries that occupy remarkable volume and (2) there exists a possibility of the accumulation of more than one crystallite forming an aggregation of particles in the solution in spite of the exposure to the ultrasonic waves [25] (Fig. 6).

3.4. Magnetic properties

Fig. 7 exhibits H–M hysteresis loops of the samples prepared via different methods and the related magnetic parameters are listed in Table 2. The squareness ratio (SQR) of the samples is

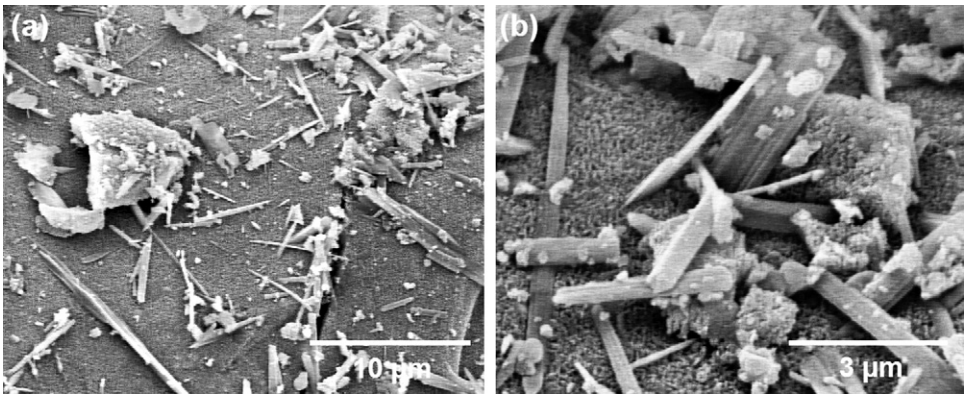

Fig. 3. SEM micrographs of $SrCo_{0.2}Fe_{11.8}O_{19}$ hexagonal ferrites prepared via co-precipitation method with different resolutions.

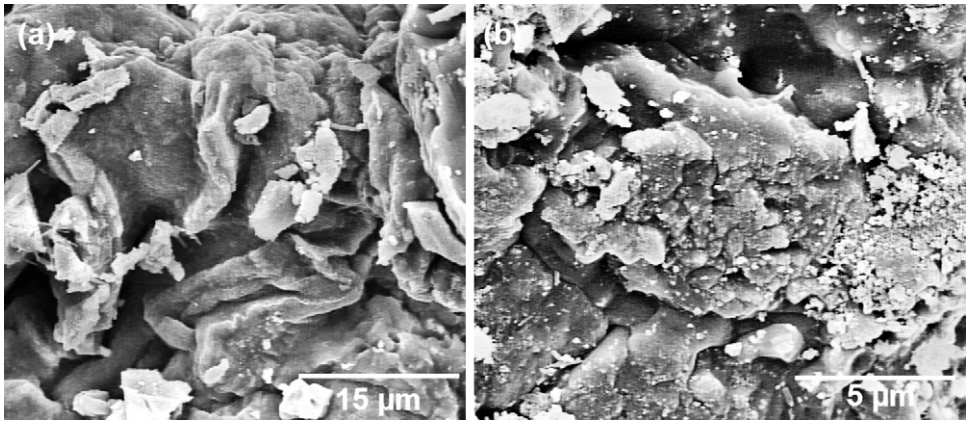

Fig. 4. SEM micrographs of $SrCo_{0.2}Fe_{11.8}O_{19}$ hexagonal ferrites prepared via sol–gel combustion route with different resolutions.

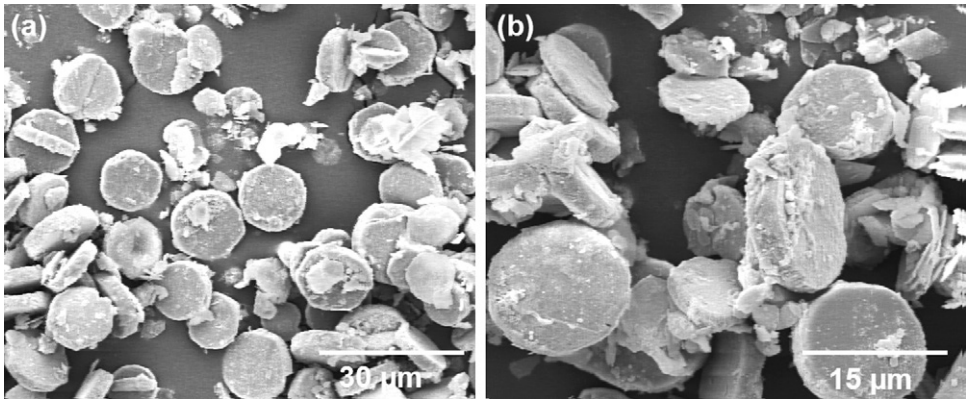

Fig. 5. SEM micrographs of $SrCo_{0.2}Fe_{11.8}O_{19}$ hexagonal ferrites prepared via hydrothermal technique with different resolutions.

denoted by the ratio Mr/Ms. The value is fundamentally a measure of squareness of the hysteresis loop. Generally, large SQR value is favoured in many applications such as magnetic recording media of high density and permanent magnets [36]. It is assumed that in co-precipitation method, the dominant factor for improving the magnetization values was attributed to the development of the $SrFe_{12}O_{19}$ phase, as supported by the XRD analysis. On the other hand, the presence of considerable amounts of α-Fe_2O_3 and $SrFe_2O_4$, which are the canted antiferromagnets, is the main cause for the low magnetic properties in sample SG which is entirely in agreement with XRD analysis. However, traces of $SrFe_2O_4$ phase still remained

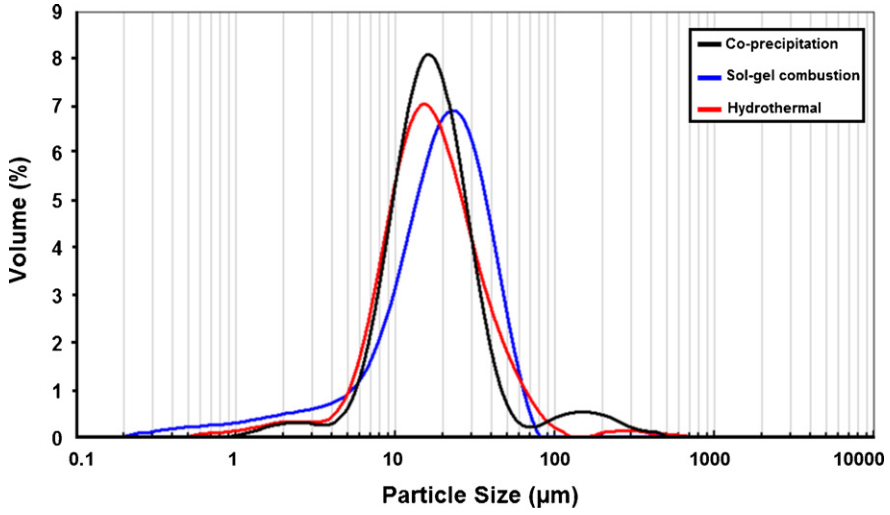

Fig. 6. Particle size distributions of $SrCo_{0.2}Fe_{11.8}O_{19}$ hexagonal ferrites produced by different methods.

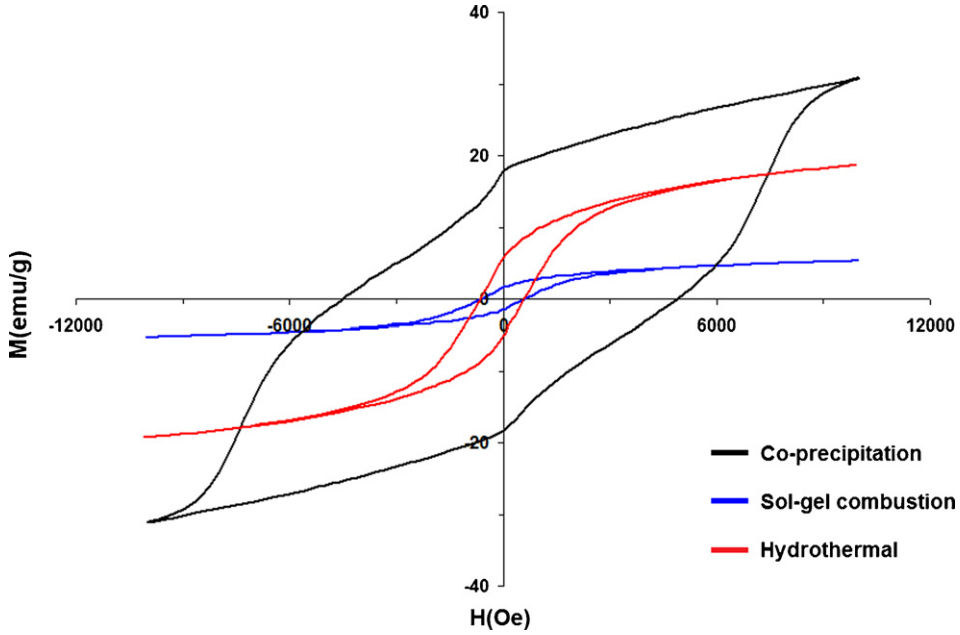

Fig. 7. Magnetic hysteresis loops of $SrCo_{0.2}Fe_{11.8}O_{19}$ hexagonal ferrites synthesized via various methods.

in the sample HT. In addition to phase deficiencies, it is worthwhile to investigate the relation between average crystallite size and magnetic properties. According to the both of tables, the saturation magnetization increases with increase in crystallite size in consequence of the growth of magnetic domains with the increase of crystalline sizes. The single magnetic domain is changed to multi-magnetic domains accompanied with the growth of magnetic domains, so the Ms of the nanocrystals are raised. The reduction of the magnetization of the magnetic particles with the decreasing particle size can be caused due to the incomplete coordination of atoms on the particle surface leading to a noncollinear spin configuration which causes the formation of a surface spin canting which might decrease the magnetization of particles [37,38]. The decrease of the saturation magnetization in parallel with the decrease in the particle size of the magnetic particles is a generally known phenomenon and is a consequence of many factors. One is certainly the large surface area of the particles and the incomplete coordination of atoms at the particle surface leading to a noncollinear spin configuration, which reduces the magnetization of small particles [39]. The second reason is connected to the energy of the magnetic particles, which depends, in an external field, on the size of the particles via the number of magnetic molecules in a single magnetic domain. This has a consequence that the thermal energy, i.e., the thermal fluctuation, will significantly weaken the total magnetic moment at a given magnetic field [40].

Consequently, the best magnetic properties are obtained by the CP route. It has been attested that the Hc of ferrites is strongly affected by grain or particle sizes [2,3,41] and may reach a maximum value during the single magnetic domain or multi-magnetic domain stages of structure [42]. In M-type strontium hexaferrite, the magnetic easy axis lies within the basal plane. The demagnetizing factor in a disk shape for a $SrFe_{12}O_{19}$ particle increases with the increase of width to thickness ratio, which leads to a drop in the coercivity [43]. Admittedly, the regular hexagonal plate-like morphology as shown in Fig. 3 leads to lower coercivity in comparison with the value obtained for CP sample. The low coercivities of the synthesized platelet crystals indicate soft magnetic behavior, which is a consequence of the large shape anisotropy (the platelet crystals are highly anisotropic) and the nucleation of domain walls, also known as the Brownian paradox [44,45]. Eventually, the low magnetization values for HT and SG samples could be the outcome of the moderately wide particle size distribution, where there is a small fraction of super-paramagnetic particles contributing to reduce magnetization consistent with the PSD results.

Table 2
Magnetic characteristics of produced Co-substituted strontium hexagonal ferrites prepared by alternative routes.

Sample	Ms (emu/g)	Mr (emu/g)	Mr/Ms	Hc (Oe)
SG	5.3	1.6	0.30	669
HT	18.3	6.6	0.36	683
CP	31.2	17.9	0.57	4950

4. Conclusions

Cobalt-substituted strontium hexagonal ferrite nanocrystallites have been synthesized successfully by the citrate sol–gel combustion, hydrothermal and co-precipitation techniques. The results indicated that the crystallographic properties of ferrite materials are extremely sensitive to the preparation route. The XRD study showed that the average particle size was found to be in the range 44–53 nm and that the M-type hexaferrite phase prepared by co-precipitation technique was single phase. However, the formed SrM ferrite phase by SG and

HT methods contained some impurity peaks, which are both α-Fe_2O_3 and $SrFe_2O_4$ phases and $SrFe_2O_4$ phase, respectively. Furthermore, Co–strontium hexaferrite nanocrystallites have been prepared with narrow particle-size distribution using the co-precipitation technique, while the products prepared by hydrothermal and sol–gel combustion routes exhibited wider particle-size distribution and less homogeneity correspondingly. The correlation of microstructure and magnetic property can be clarified by means of SEM analysis and variable morphologies like lamellar, disk-like and needle-shaped were observed from SG, HT and CP sample's micrographs. Moreover, the shape of the hysteresis loop curves confirmed that the CP hexagonal ferrite was a hard magnet. In contrast, the low saturation magnetization (Ms) for SG and HT samples was attributed to the purity, the particle size effects and the surface spin-canting phenomenon. The results demonstrate that the coercivity of fine powders is lower than that of the larger prepared by co-precipitation route which led to obtain softer magnets by hydrothermal and sol–gel combustion methods. Compare to the other mentioned methods, the chemical co-precipitation method is a low cost technique suitable for the mass production. From our results it is confirmed that the magnetic properties of strontium hexaferrite are very much affected by altering the synthesis route. The findings in this study are believed to provide further insights to understanding of the correspondence between the magnetic properties of $SrCo_{0.2}Fe_{11.8}O_{19}$ nanocrystals and the kind of synthesis route.

Acknowledgements

The authors would like to acknowledge Iran National Science Foundation (INSF) and Color &Polymer Research Center (CPRC) for helping us in this project.

References

[1] N.A. Spaldin, Magnetic Materials, 1st ed., Cambridge University Press, Cambridge, 2010.
[2] R. Valenzuela, Magnetic Ceramics, Cambridge University Press, Cambridge, 1994.
[3] A. Goldman, Modern Ferrite Technology, 2nd ed., Springer, Pitsburgh, 2006.
[4] M. Robbins, E. Banks, Effect of fluoride-compensated Co^{2+} on the anisotropy of $BaFe_{12}O_{19}$, J. Appl. Phys. 34 (1963) 1260–1261.
[5] T.S. Chin, M.C. Deng, S.L. Hsu, C.H. Lin, (Ni,Ti), (Ni,Sn) and (Zn,Ti) substituted barium ferrite particles prepared by a flux method with δ-FeOOH as a precursor, IEEE Trans. Magn. 30 (1994) 4110–4112.
[6] X. Zhang, Y. Yu, M. Duan, M. Guillot, An investigation on the magneto-optical enhancement in Ni-substituted barium ferrites, J. Appl. Phys. 79 (1996) 5979–5981.
[7] X. Battle, M. Garcia del Muro, J. Tejada, H. Pfeiffer, P. Gornert, E. Sinn, Static magnetic properties of nanocrystalline Co-Ti doped barium ferrite $BaFe_{12-2x}Co_xTi_xO_{19}$ ($x = 0.8$), IEEE Trans. Magn. 30 (1994) 708–710.
[8] M. Kishimoto, S. Kitahata, M. Amemiya, Effect of magnetic anisotropy of Ba-ferrite particles on squareness of perpendicular recording media, J. Appl. Phys. 61 (1987) 3875–3877.
[9] G. Mendoza-Suarez, L.P. Rivas-Vazquez, J.C. Corral-Huacuz, A.F. Fuentes, J.I. Escalante Garcia, Magnetic properties and microstructure of $BaFe_{11.6-2x}Ti_xM_xO_{19}$ (M = Co, Zn, Sn) compounds, Physica B 339 (2003) 110–118.
[10] G.B. Teh, D.A. Jefferson, High-resolution transmission electron microscopy studies of sol–gel-derived cobalt-substituted barium ferrite, J. Solid State Chem. 167 (2002) 254–257.
[11] Z. Simsa, S. Lego, R. Gerber, E. Pollert, Cation distribution in Co–Ti-substituted barium hexaferrites: a consistent model, J. Magn. Magn. Mater. 140 (1995) 2103–2104.
[12] G. Wiesinger, M. Müller, R. Grössinger, M. Pieper, A. Morel, F. Kools, P. Tenaud, J.M. Le Breton, J. Kreisel, Substituted ferrites studied by nuclear methods, J. Phys. Stat. Sol. A 189 (2002) 499–508.
[13] L. Lechevallier, J.M. Le Breton, A. Morel, P. Tenaud, Influence of the presence of Co on the rare earth solubility in M-type hexaferrite powders, J. Magn. Magn. Mater. 316 (2007) 109–111.
[14] Y. Liu, M.G.B. Drew, Y. Liu, Preparation and magnetic properties of barium ferrites substituted with manganese, cobalt, and tin, J. Magn. Magn. Mater. 323 (2011) 945–953.
[15] R. Carey, P.A. Gago Sandoval, D.M. Newman, B.W.J. Thomas, The magnetic and magneto-optical properties of Co, Cr, Mn, and Ni substituted barium ferrite films, J. Appl. Phys. 75 (1994) 6789–6791.
[16] X. Battle, X. Obradors, J. Rodrıguez Carvajal, M. Pernet, M.V. Cabanas, M. Vallet, Cation distribution and intrinsic magnetic properties of Co-Ti-doped M-type barium ferrite, J. Appl. Phys. 70 (1991) 1614–1623.
[17] X. Battle, M. Garcia del Muro, J. Tejada, H. Pfeiffer, P.G. ornert, E. Sinn, Magnetic study of M-type doped barium ferrite nanocrystalline powders, J. Appl. Phys. 74 (1993) 3333–3340.
[18] C.P. Liu, M.W. Li, Z. Cui, J.R. Huang, Y.L. Tian, T. Lin, W.B. Mi, Comparative study of magnesium ferrite nanocrystallites prepared by sol–gel coprecipitation methods, J. Mater. Sci. 42 (2007) 6133–6138.
[19] F.J. Berry, J.F. Marco, C.B. Ponton, K.R. Whittle, Preparation and characterization of rare earth-doped strontium hexaferrites $Sr_{1-x}M_xFe_{12}O_{19}$ (M = La, Eu), J. Phys. Chem. Solids 20 (2001) 431.
[20] A. Mali, A. Ataie, Influence of the metal nitrates to citric acid molar ratio on the combustion process and phase constitution of barium hexaferrite particles prepared by sol–gel combustion method, J. Ceram Int. 30 (2004) 1979–1983.
[21] H.Y. He, Comparison study on magnetic property of $Co_{0.5}Zn_{0.5}Fe_2O_4$ powders by template-assisted sol–gel and hydrothermal methods, J. Mater. Sci. Mater. Electron. (2011), doi:10.1007/s10854-011-0535-2.
[22] P. Xu, X. Han, M. Wang, Synthesis and magnetic properties of $BaFe_{12}O_{19}$ hexaferrite nanoparticles by a reverse microemulsion technique, J. Phys. Chem. C 111 (2007) 5866–5870.
[23] A. Ataie, A. Mali, Characteristics of barium hexaferrite nanocrystalline powders prepared by a sol–gel combustion method using inorganic agent, J. Electroceram. 21 (2008) 357–360.
[24] M.M. Rashad, I.A. Ibrahim, Improvement of the magnetic properties of barium hexaferrite nanopowders using modified co-precipitation method, J. Magn. Magn. Mater. 323 (2011) 2158–2164.
[25] M.K. Elnimr, B.M. Moharram, S.A. Saafan, S.T. Assar, Particle size distribution, magnetic permeability and dc conductivity of nano-structured and bulk LiNiZn-ferrite samples, J. Magn. Magn. Mater. 322 (2010) 2108–2112.
[26] R.H. Arendt, The molten salt synthesis of single magnetic domain $BaFe_{12}O_{19}$ and $SrFe_{12}O_{19}$ crystals, J. Solid State Chem. 8 (1973) 339–347.
[27] C. Singh, S. Bindra, I.S. Hudiara, Y. Bai, K. Marina, Hystersis analysis of Co–Ti substituted M-type Ba–Sr hexagonal ferrite, Mater. Lett. 63 (2009) 1921–1924.
[28] C. Sun, K. Sun, Sol–gel synthesis of Ce-substituted $BaFe_{12}O_{19}$, J. Mater. Sci. 42 (2007) 5676–5679.
[29] M.M. Hessien, M.M. Rashad, M.S. Hassan, K. El-Barawy, Synthesis and magnetic properties of strontium hexaferrite from celestite ore, J. Alloys Compd. 476 (2009) 373–378.
[30] L. Du, Y.C. Du, Y. Li, J.Y. Wang, C. Wang, X.H. Wang, P. Xu, X.J. Han, Surfactant-assisted solvothermal synthesis of $Ba(CoTi)_xFe_{12-2x}O_{19}$ nanoparticles and enhancement in microwave absorption properties of polyaniline, J. Phys. Chem. C 114 (2010) 19600–19606.
[31] C. Singh, S.B. Narang, I.S. Hudiara, Y. Bai, F. Tabatabaei, Static magnetic properties of Co and Ru substituted Ba–Sr ferrite, Mater. Res. Bull. 43 (2008) 176–184.

[32] H. Mocuta, L. Lechevallier, J.M. Le Breton, J.F. Wang, I.R. Harris, Structural and magnetic properties of hydrothermally synthesised $Sr_{1-x}Nd_xFe_{12}O_{19}$ hexagonal ferrites, J. Alloys Compd. 364 (2004) 48–52.
[33] I. Capek, Preparation of metal nanoparticles in water-in-oil (w/o) microemulsions, Adv. Colloid Interface Sci. 110 (2004) 49–74.
[34] P.H. Martha, Microwave applications of soft ferrites, J. Magn. Magn. Mater. 215 (2000) 171–183.
[35] A. Verma, T.C. Goel, R.G. Mendiratta, Frequency variation of initial permeability of NiZn ferrites prepared by the citrate precursor method, J. Magn. Magn. Mater. 210 (2000) 274–278.
[36] K.K. Mallick, P. Shepherd, R.J. Green, Magnetic properties of cobalt substituted M-type barium hexaferrite prepared by co-precipitation, J. Magn. Magn. Mater. 312 (2007) 418–429.
[37] J.M.D. Coey, Noncollinear spin arrangement in ultrafine ferrimagnetic crystallites, Phys. Rev. Lett. 27 (1971) 1140–1142.
[38] R.H. Kodama, A.E. Berkowitz, E.J. McNiff, S. Foner, Surface spin disorder in $NiFe_2O_4$ nanoparticles, Phys. Rev. Lett. 77 (1996) 394–397.
[39] S. Kurisu, T. Ido, H. Yokoyama, Surface effect on saturation magnetization of Co and Ti substituted Ba-Ferrite fine particles, IEEE Trans. Magn. 23 (1987) 3137–3139.
[40] R.H. Kadama, A.E. Berkowitz, E.J.M. Niff, S. Foner, Surface spin disorder in $NiFe_2O_4$ nanoparticles, Phys. Rev. Lett. 77 (1996) 394–397.
[41] M.A. Gilleo, A handbook on the properties of magnetically ordered substances, in: P. Wohlfarth (Ed.), Ferromagnetic Materials, vol. 3, North-Holland, Amsterdam, 1982, pp. 334–342.
[42] A.S. Albuquerque, J.D. Ardisson, W.A.A. Maccdo, M. Alves, Nanosized powders of NiZn ferrite: synthesis, structure, and magnetism, J. Appl. Phys. 87 (2000) 4352–4357.
[43] E.C. Stoner, E.P. Wohlfarth, A mechanism of magnetic hysteresis in heterogeneous alloys, Philos. Trans. R. Soc. Lond. 240 (1948) 559–642.
[44] B.D. Cullity, C.D. Graham, Introduction to Magnetic Materials, 2nd ed., IEEE Press, New Jersey, 2009.
[45] J.E. Knowles, The measurement of the anisotropy field of single ‘‘tape’’ particles, IEEE Trans. Magn. 20 (1984) 84–86.